Cholesteric and Nematic Liquid Crystalline Phase Behavior of Double-Stranded DNA Stabilized Single-Walled Carbon Nanotube Dispersions

Geyou Ao,[†] Dhriti Nepal,[†] Michelle Aono,[‡] and Virginia A. Davis[†,*]

[†]Department of Chemical Engineering and [‡]College of Veterinary Medicine, Auburn University, Auburn, Alabama 36849, United States

ABSTRACT The first lyotropic cholesteric single-walled carbon nanotube (SWNT) liquid crystal phase was obtained by dispersing SWNTs in an aqueous solution of double-stranded DNA (dsDNA). Depending on the dispersion methodology, the polydomain nematic phase previously reported for other lyotropic carbon nanotube dispersions could also be obtained. The phase behavior and dispersion microstructure were affected by the relative concentrations of dsDNA and SWNT and whether small bundles were removed prior to concentrating the dispersions. This readily controlled phase behavior opens new routes for producing SWNT films with controlled morphology.

KEYWORDS: single-walled carbon nanotubes · double-stranded DNA · cholesteric liquid crystal · phase behavior

Large area assemblies of single-walled carbon nanotubes (SWNTs) have numerous potential applications including strong antimicrobial coatings,[1−3] artificial muscles,[4] chemical sensors,[5,6] electrical wires,[7,8] and high strength fibers.[9−13] However, translating the remarkable mechanical, thermal, and electrical properties of individual SWNTs into macroscopic objects is hindered by the strong van der Waals attraction between SWNTs and the random entanglements resulting from many synthesis schemes. Lyotropic liquid crystalline SWNT dispersions are recognized as a key potential precursor for the fluid phase processing of carbon nanotubes into aligned materials with outstanding properties.[9] Several research groups have achieved lyotropic carbon nanotube liquid crystalline phases; however, they have all been polydomain nematics.[14−19] While shear and other forces applied during processing can be used to anneal defects between domains, it has been shown that dispersions with larger domain size and fewer defects result in fewer defects in the assembled solid material.[19] The lack of a smooth liquid crystal microstructure in most systems has been deemed a key impediment to producing macroscale materials with outstanding properties.[20] Furthermore, while nematic liquid crystalline phases are useful for producing aligned films and fibers, the inability to produce cholesteric SWNT dispersions has limited the range of potential applications. An inherent property of the cholesteric microstructure is the selective reflection of visible light; there is growing interest in using films produced from cholesteric phases in security papers and passive optical devices such as circular polarizers, notch filters, and reflective displays.[21,22] The majority of cholesteric film research to date has focused on cellulose nanowhiskers; until now, it has not been possible to achieve this microstructure with SWNTs.

In parallel to the ongoing advancements in bottom-up assembly of liquid crystalline nanocylinder (*e.g.*, nanotubes, nanowires, nanowhiskers) dispersions,[23] there has been growing interest in dispersing carbon nanotubes in solutions of biological molecules such as DNA and enzymes. These materials are some of the best known dispersants for carbon nanotubes due to their amphiphobic nature and potential for $\pi-\pi$ interactions;[1,24,25] they also offer the advantages of green chemistry, potential biocompatibility, and multifunctionality. Pioneering work by the Poulin group demonstrated that evaporation of low concentration dispersions of SWNTs in single-stranded DNA (ssDNA)[15] and hyaluronic acid (HLA)[16] resulted in liquid crystalline phase formation. In addition, Hobbie *et al.* have shown that SWNTs dispersed in bile salts can be assembled into fibrils as a result of the mesogenic nature of the solvent and geometrical confinement.[26] It is noteworthy that, in addition to enabling carbon nanotube dispersion,

*Address correspondence to davisva@auburn.edu.

Received for review November 26, 2010 and accepted January 12, 2011.

Published online January 28, 2011
10.1021/nn103225r

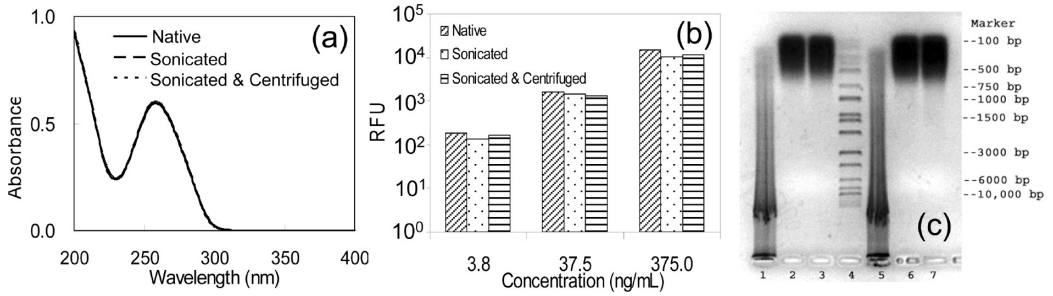

Figure 1. (a) UV−vis absorbance spectra using a 1 mm path length quartz cell for a 1:20 dilution of 0.44 vol % dsDNA aqueous solutions before sonication (native), after sonication, and after both sonication and centrifugation. (b) Fluorescence of successive dilutions of dsDNA solutions using picogreen. (c) Agarose gel electrophoresis of dsDNA solutions: (1) 7.5 μg of dsDNA before sonication, (2) after sonication, (3) after sonication/centrifugation, (4) 10 μL of HiLo dsDNA marker (Bionexus) and (5) 15 μg of dsDNA before sonication, (6) after sonication, (7) after sonication/centrifugation.

many biological molecules are themselves mesogenic. For example, tobacco mosaic virus (TMV) was the material used in Onsager's original work on liquid crystalline phase formation.[27] More recently, the rod-like bacteriophage *fd* virus has been studied as a model system; this research includes fascinating work examining the phase behavior of dispersions containing both rods and spheres.[28,29] In addition, the long and stiff helical structure of dsDNA molecules enables formation of multiple liquid crystalline phases;[30,31] the critical concentration for cholesteric formation depends on factors such as the number of dsDNA base pairs and the ionic strength.[30−33] Cholesteric liquid crystalline phases of dsDNA are even evidenced to form *in vivo*.[34−36]

In this work, we compare the phase behavior of dsDNA/SWNT dispersions produced by two different methods. Evaporation of bulk dispersions, composed of both bundled and individual SWNTs, resulted in nematic phase formation, while evaporation of dsDNA/SWNT supernatants resulted in cholesteric phase formation. To our knowledge, this is the first lyotropic cholesteric SWNT liquid crystal. The origin of the cholesteric structure can be directly attributed to the majority of the dsDNA retaining its helical structure during processing. This structure can be retained or eliminated during processing into aligned films. The potential enhanced biocompatibility of dsDNA/SWNT and the previously never achieved cholesteric microstructure suggest that the range of applications that can be processed from liquid crystalline nanotube dispersions may be even broader than previously thought.

RESULTS AND DISCUSSION

The majority of DNA/SWNT dispersion research to date has been performed using ssDNA. Similar to the dispersion of SWNTs in ssDNA, dispersion of SWNTs in dsDNA requires sonication; this results in high localized temperatures and shear. In this work, an ice bath was used to prevent significant heating of the bulk dispersion. In order to investigate whether sonication and/or subsequent centrifugation affected the dsDNA structure, we analyzed solutions of dsDNA before and after these processing steps using fluorescence spectroscopy and gel electrophoresis. The absorbance ratio at 260 and 280 nm was determined for the dsDNA raw material. This is a typical test for purity; the measured ratio A_{260}/A_{280} = 1.86 was in the range of 1.8−2.0, which is generally considered an indication of pure dsDNA.[37] Solutions of 0.44 vol % (0.75 wt %) dsDNA in deionized water were characterized before sonication, after sonication, and after both sonication and centrifugation. As shown in Figure 1a, the absorbances of all three DNA solutions were almost identical. Since the hyperchromicity of ssDNA results in a 40% increase in absorbance relative to dsDNA,[37] the absence of any change in the absorbance spectra supports that the solutions contained primarily dsDNA. Furthermore, for several concentrations of each solution, fluorescence spectroscopy was performed using picogreen, which preferentially binds to dsDNA.[38] If the processing was creating a large amount of ssDNA, a large decrease in the picogreen relative fluorescence units (RFU) would be expected, but this was not observed (Figure 1b). However, as shown in Figure 1c, sonication did significantly shorten the dsDNA from over 10 000 base pairs into pieces less than 750 base pairs (<0.255 μm) in length.

The phase behavior of dispersions of 1.0 wt % dsDNA/0.10 wt % SWNTs (10.0:1.0), 0.75 wt % dsDNA/0.10 wt % SWNTs (7.5:1.0), and 0.50 wt % dsDNA/0.10 wt % SWNTs (5.0:1.0) were investigated using cross-polarized microscopy and rheology. On the basis of a SWNT density of 1.45 g/cm^3, dsDNA density of 1.70 g/cm^3, and a water density of 1.00 g/cm^3, these ratios corresponded to 0.59 vol % dsDNA/0.07 vol % SWNTs (8.5:1.0), 0.44 vol % dsDNA/0.07 vol % SWNTs (6.4:1.0), and 0.29 vol % dsDNA/0.07 vol % SWNTs (4.3:1.0). In addition to studying the phase behavior of the bulk dispersions, dispersions of 0.44 vol % dsDNA/0.07 vol % SWNT were centrifuged at 17 000*g* to remove bundles, and the resulting supernatants of individual SWNTs[1] were evaporated. Interestingly, repeated thermogravimetric analyses and mass balances

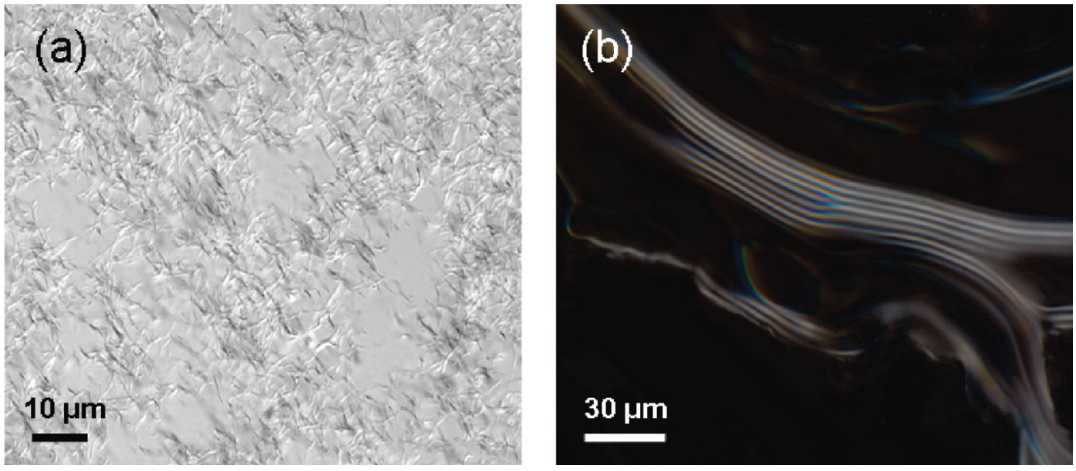

Figure 2. dsDNA/SWNT dispersions of (a) 13.6:1.0 by volume dsDNA/SWNT (15.9:1.0 by weight) without centrifugation at a SWNT concentration of 0.24 vol % and (b) supernatant of 4.4:1.0 by volume dsDNA:SWNT at a SWNT concentration of 0.69 vol % under cross-polarized light.

on various concentrations of centrifuged dsDNA/SWNT samples showed that the dsDNA/SWNT volume ratio decreased from 6.4:1.0 to 4.4:1.0 (weight ratio of 5.1:1.0) in the supernatant.

Similar to the findings of Badaire *et al.*[15] for ssDNA/SWNT, the phase behavior of the bulk (noncentrifuged) dispersions was dependent on the dsDNA/SWNT ratio; if insufficient dsDNA was present to stabilize the SWNTs, increasing concentration resulted in aggregate formation. In this work, evaporation of a dispersion of 1.0:1.0 dsDNA/SWNT by weight (0.85:1.0 by volume) resulted in the formation of visible aggregates tens to hundreds of micrometers in diameter due to the presence of an insufficient amount of dsDNA to counteract the inherent 20−40 k_BT/nm[39,40] van der Waals attraction between SWNTs. In contrast, Badaire *et al.* (2005) observed sufficient stabilization to enable liquid crystalline phase behavior for 1:1 by weight dispersions of ssDNA/SWNT. Since impurities are known to stabilize SWNT dispersions by creating physical impediments to reagglomeration, this discrepancy is largely attributed to the present work using SWNT batches with purity ranging from 92.0% to 99.7%, while Badaire *et al.* used SWNTs with 80% purity.[15] Differences between the type of DNA, the dispersion preparation, and the SWNT size distribution and surface chemistry also likely contributed to differences in phase behavior.

Evaporation of the dispersions containing an excess of dsDNA resulted in the phase behavior typical of dispersions of rods.[41] The dispersions were isotropic at low concentration. With increasing concentration (evaporation), the systems became biphasic (a liquid crystalline phase formed in equilibrium with the isotropic phase). The fraction of birefringent liquid crystal domains increased with concentration until the systems became completely liquid crystalline at a critical volume fraction designated ϕ_{LC}. Figure 2a shows that, in the biphasic region, these dispersions exhibited strand-like spaghetti structures similar to that observed for SWNTs in superacids.[18] These strands are nematic liquid crystalline domains where the SWNTs are free to translate along the length of the strands. In contrast to the bulk dispersions, the initial birefringent morphology for the dsDNA/SWNT supernatants was narrow moving streams of near-parallel lines indicative of the initial stage of cholesteric liquid crystal formation (Figure 2b).

As shown in Figure 3, the differences in morphology between the concentrated bulk dispersions and concentrated supernatants became even more dramatic at higher concentrations. The polydomain nematic structure shown in Figure 3a for a concentrated bulk (noncentrifuged) dispersion of 4.3:1.0 dsDNA/SWNT at a concentration of 1.7 vol % SWNTs has a similar microstructure to that previously observed for liquid crystals of SWNT/102% H_2SO_4,[18,19] MWNTox/H_2O,[14,42] and ssDNA/SWNT.[15] The SWNTs were locally aligned within each domain but are randomly oriented on a larger length scale. The individual domains became bright and dim as the samples were rotated between cross-polarizers (see Supporting Information for additional images). For these dispersions, the critical concentration ϕ_{LC} for the biphasic to liquid crystal transition depended on the initial dsDNA/SWNT ratio. Cross-polarized optical microscopy was initially used to approximate this transition by determining the lowest concentration at which no isotropic domains were observed. Since this method is somewhat dependent on the magnification and the concentrations tested, rheology was also used for further confirmation of liquid crystalline phase behavior and to substantiate the estimated value of ϕ_{LC}. In a normal polymer solution or colloidal dispersion, the low shear viscosity increases with concentration. However, for liquid crystalline dispersions, viscosity does not change monotonically with increasing concentration. The

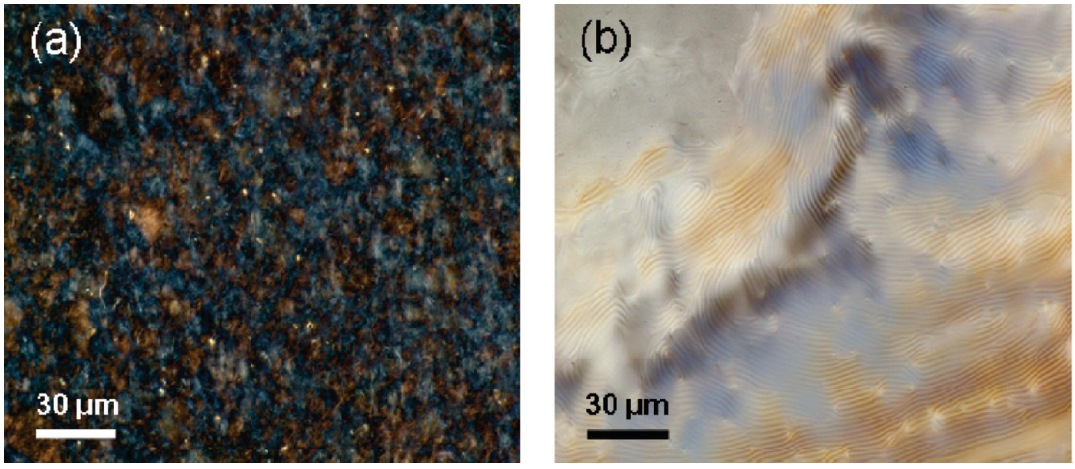

Figure 3. Comparison of dsDNA/SWNT dispersions of (a) noncentrifuged 4.3:1.0 by volume dsDNA/SWNT at a SWNT concentration of 1.7 vol % SWNT and (b) supernatant of 4.4:1.0 by volume dsDNA/SWNT at 2.3 vol % SWNT under cross-polarized light.

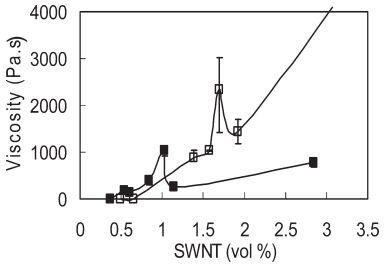

Figure 4. Relationship between viscosity and concentration at a shear rate of 0.1 s^{-1} and a temperature of 10 °C for bulk (noncentrifuged) dsDNA/SWNT dispersions obtained from 8.5:1.0 (solid squares) and 4.3:1.0 (open squares) dsDNA/SWNT by volume. Error bars are given for all points but are smaller than the data markers in many cases. The largest error bars are in the biphasic region at the peak in viscosity; this is consistent with previous research on lyotropic rod-like polymers and SWNTs in superacids.

viscosity increases with concentration as long as the system is predominantly isotropic. However, the increasing fraction of anisotropic domains eventually results in a decreased resistance to flow. Viscosity therefore decreases with concentration until increasing rod concentration no longer results in increased order. Once the order can no longer be increased, the viscosity once again increases with concentration. Therefore, in the biphasic region, the viscosity *versus* concentration curve goes through a maximum and then reaches a minimum at approximately ϕ_{LC}. On the basis of the minima shown in Figure 4, bulk dispersions evaporated from a 8.5:1 dsDNA/SWNT have $\phi_{LC} \sim 1.2$ vol %, while those from 4.3:1.0 dsDNA/SWNT have $\phi_{LC} \sim 1.9$ vol %. This may indicate the presence of more bundles in the 4.3:1.0 dsDNA/SWNTs since a lower average aspect ratio would result in a higher value of ϕ_{LC}.

As shown in Figure 3b, the liquid crystal formed by concentrating the dsDNA/SWNT supernatants has a dramatically different microstructure than previously obtained lyotropic SWNT liquid crystals. The classical fingerprint texture[43] consisting of dark and light strips under a cross-polarized light microscope indicates a cholesteric structure in which the molecules are respectively normal to, and in the plane of, the polarizer.[32,43] Figure 5 shows the evolution of the cholesteric microstructure and dispersion viscosity with increasing concentration (additional images in Supporting Information). A cholesteric oily streak texture of thin near-parallel lines started to appear at 0.69 vol % of SWNTs (3.6 vol % dsDNA) due to the amount of excess, or free, dsDNA which was not strongly interacting with the SWNTs. Large birefringent domains were observed at 1.5 vol % SWNTs, where the viscosity was at its maximum value of 2165 Pa·s. Still further increasing the concentration resulted in the domains of near-parallel set of swirling lines growing larger and the appearance of many compactly distributed small spherical swirling lines resembling fish scales. Areas without obvious fingerprint textures resembled oil paint and also exhibited strong birefringence under polarized light. Further increasing concentration resulted in extending birefringent domains; iridescent colors appeared at the concentrations near the viscosity minimum at 2.2 vol % SWNT. Moreover, when the polarizer was extracted, all of these textures disappeared and the sample was a uniform gray. This indicated uniform dispersion throughout the sample without any noticeable aggregates or clusters. When rotating the specimens relative to the polarizers, different domains of the cholesteric phases changed colors, resulting in white, beige, orange, purple, light green, and blue regions. This was due to pseudo-Bragg reflections, which are one of the characteristic optical properties of a cholesteric phase.[43] The color variation became more obvious with increasing concentration

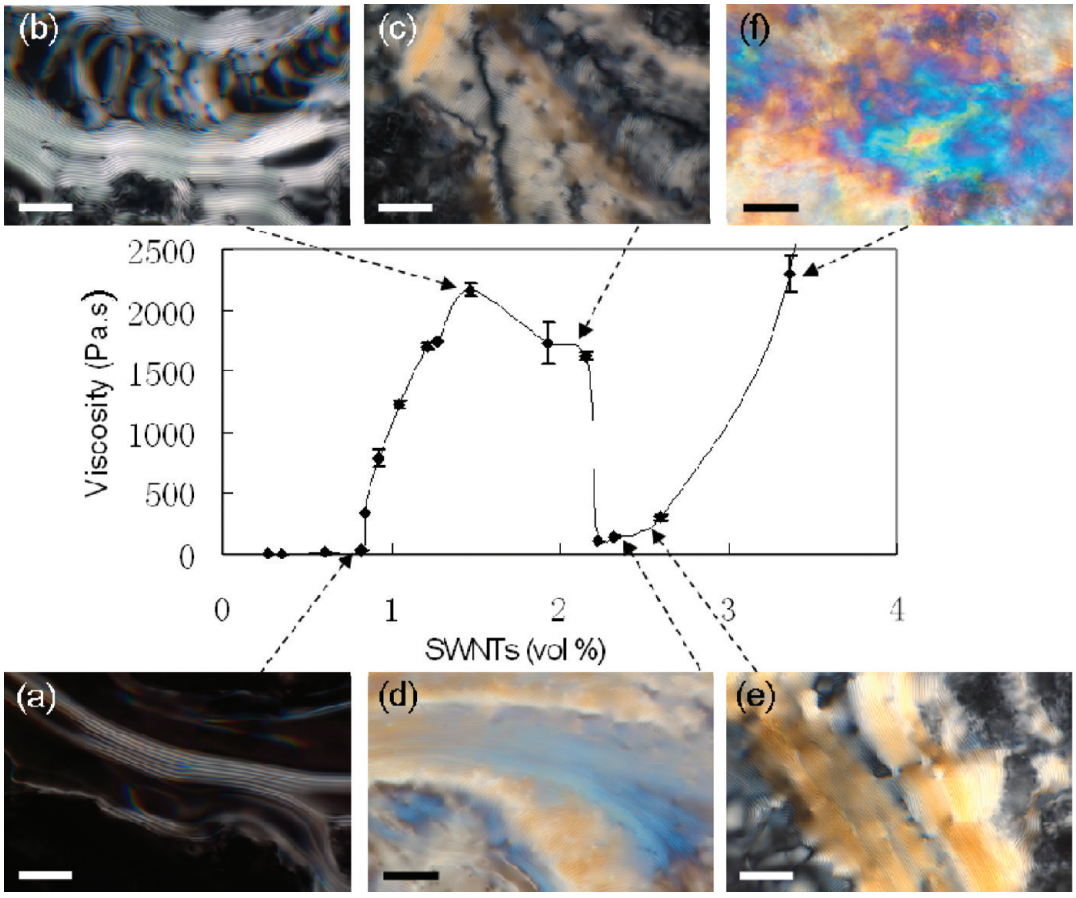

Figure 5. Relationship between viscosity and concentration for concentrated supernatants of 4.4:1 by volume dsDNA/SWNT at a shear rate of 0.1 s^{-1} and temperature of 10 °C. Images were taken under cross-polarized light. The SWNT concentrations were (a) 0.69 vol %, (b) 1.5 vol %, (c) 2.0 vol %, (d) 2.3 vol %, (e) 2.5 vol %, and (f) 3.4 vol %. The scale bars are 30 μm.

in response to variations in the helical pitch. The pitch of the dsDNA/SWNT dispersions decreased linearly from 3.45 ± 0.25 to 2.65 ± 0.15 μm when the concentration of SWNTs increased from 1.2 to 2.0 vol %; this is in the transition range from the biphasic region to single-phase liquid crystal and indicates a more ordered alignment of molecules in the cholesteric phase with increasing concentration. With a further increase in concentration to 2.9 vol %, the pitch increased to 3.38 ± 0.53 μm. At even higher concentrations, the fingerprint texture was absent due to the development of a more solid-like phase; this is supported by a plateau in rheological measurements of storage modulus *versus* frequency for these dispersions.

The surprising difference between the microstructures obtained from concentrated bulk dispersions and concentrated supernatants is related to the cholesterogenic nature of dsDNA (Figure 6a) and the initial dispersion state of the SWNTs. Aqueous dsDNA solutions prepared by the same procedure, but without the addition of SWNTs, exhibited cholesteric phase behavior. They became biphasic at 6.2 vol % and fully liquid crystalline at $\phi_{LC} \sim 12.6$ vol %. These values are markedly higher than those obtained in the presence of SWNTs; this indicates that the presence of the higher aspect ratio more rigid SWNTs facilitated liquid crystalline phase formation. The pitch of the dsDNA solutions monotonically decreased from 4.35 ± 0.38 to 3.02 ± 0.20 μm, while the concentration increased from 8.1 to 19.3 vol %; these values are slightly higher than those for the concentrated dsDNA/SWNT. The structure and pitch of DNA cholesterics are dependent on many factors such as the molecular length of DNA fragments, interaxial spacing of molecules, and solvent conditions such as osmotic pressure and ionic strength. In addition, steric, van der Waals, and hydration forces may also contribute to macroscopic properties of DNA cholesterics.[44−46]

In the presence of SWNTs, there appears to be a competition between the tendency of the dsDNA to form a cholesteric liquid crystal and the tendency of the SWNTs to form a nematic liquid crystal. When the initial dispersion is a dsDNA/SWNT supernatant consisting of individual SWNTs,[1] the natural tendency of dsDNA to form cholesteric phases dominates; this indicates that the majority of dsDNA retains its helicity over time. The majority of bulk dispersions exhibited the previously described polydomain nematic texture that has been characteristic of all lyotropic carbon

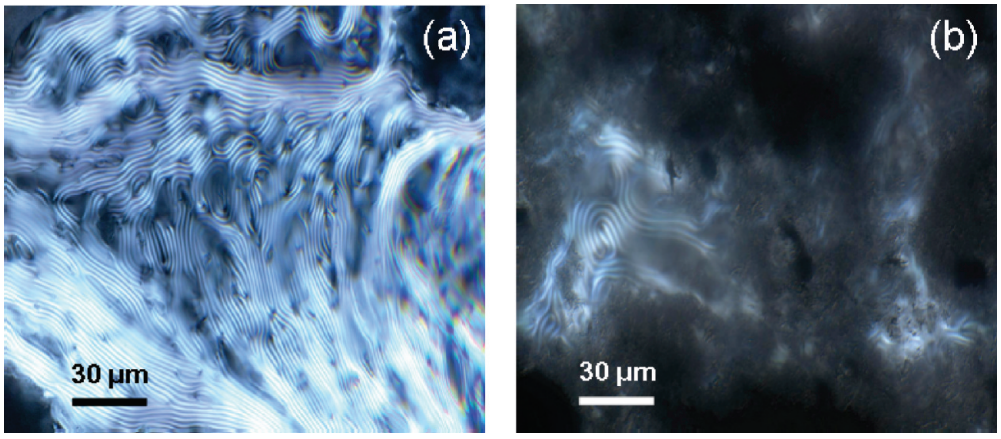

Figure 6. Fingerprint texture in (a) 19.3 vol % of dsDNA solution and (b) bulk 6.4:1.0 by volume dsDNA/SWNT dispersion at a SWNT concentration of 1.3 vol %.

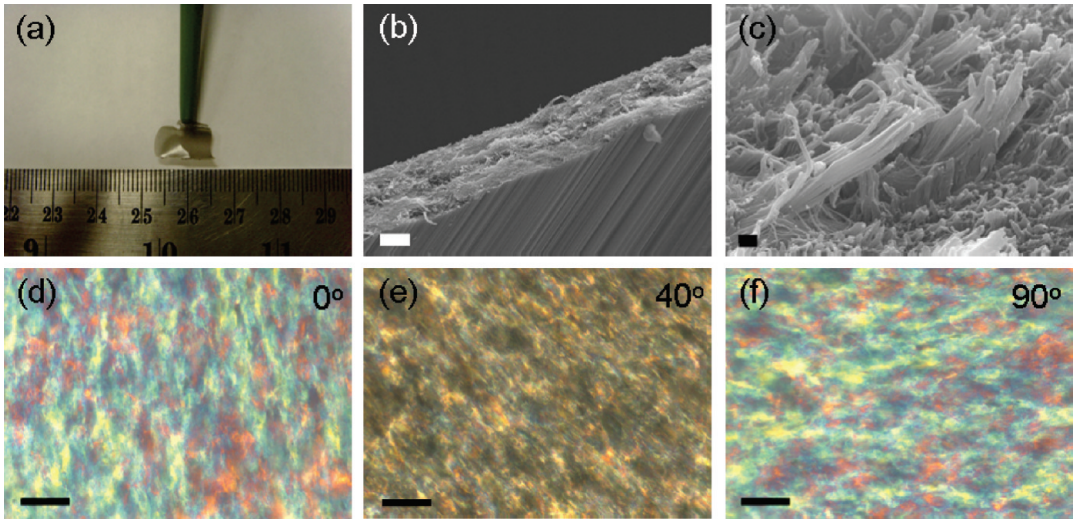

Figure 7. (a) Translucent film obtained from a 4.4:1.0 by volume supernatant of dsDNA/SWNT dispersion (~2.0 vol % of SWNTs) by shearing at approximately 500 s^{-1} and (b,c) corresponding SEM images. (d−f) Cross-polarized optical microcopy images of films prepared without applied shear. The colors vary as the sample is rotated in (d) 0°, (e) 40°, and (f) 90°. The scale bars are (b) 10 μm, (c) 200 nm, and (d−f) 50 μm.

nanotube liquid crystals to date. However, in the case of some bulk dsDNA/SWNT dispersions, such as the 6.4:1.0 dispersion concentrated to 1.3 vol % shown in Figure 6b, small fingerprint regions were observed due to the excess amount of free dsDNA. However, these small regions did not form continuous domains and were not visible at higher concentration. We believe that, in the bulk dispersions, the presence of SWNT bundles physically impedes the formation of continuous cholesteric domains. In addition, Cathcart *et al.*[47] have suggested that dsDNA denatures in the process of debundling SWNTs over a time period of approximately 30 days. Therefore, the presence of SWNT bundles in the bulk dispersion may result in some dsDNA denaturation during the evaporation process and a reduction in the driving force for cholesteric phase formation.

It has previously been shown that processing nematic liquid crystalline dispersions is a promising route for producing aligned solid materials such as films and fibers.[9,10,19,48] Considerably less is known about processing lyotropic cholesteric dispersions.[49] Research on cellulose nanowhisker liquid crystals has shown that retention of helicity during processing can enable films with controllable optical properties that can be used for such circular polarizers, reflective displays, and security papers.[21,22] Spreading cholesteric dsDNA/SWNT dispersions (2.0 vol % SWNT) onto copper tape by roller coating, allowing the coating to dry, and removing the substrate resulted in approximately 20 μm thick films which were translucent over ambient light (Figure 7a). Under cross-polarized light, they appeared either bright or dark depending on the orientation of the polarizer. SEM of these films (Figure 7b,c) revealed an aligned densely packed structure composed of dsDNA/SWNT bundles ranging from 8 to 22 nm in diameter; the alignment and packing in this microstructure is far superior to our

previously reported aligned dsDNA/SWNT films produced from dilute dispersions using layer-by-layer assembly and directed air stream drying.[1] These results may indicate the shear applied during processing induced in a cholesteric to nematic transition such as that previously proposed for rod-like polymer solutions. Since the effects of shear on cholesteric liquid crystals are not as well understood as the effects of shear on nematic liquid crystals, future rheo-optical characterization and theoretical modeling of this system may provide new insights into the shear induced unwinding of cholesteric phases into nematic phases. Producing the films by simply dropping the cholesteric dispersions onto the tape and not applying any shear also resulted in materials that were translucent under ambient light. However, under cross-polarized light, these films showed bright birefringent bands indicative of the retention of cholesteric structure (Figure 7d–f). These films are similar in appearance to those obtained by Lee *et al.*[50] for films produced from a helical liquid crystalline phase of Au-antistreptavidin M13 virus.

CONCLUSION

When dsDNA/SWNT liquid crystals were produced from a bulk dispersion, the presence of SWNT bundles appeared to inhibit cholesteric phase formation; this resulted in the nematic texture typical of other SWNT liquid crystals. When the liquid crystal was produced from a supernatant composed only of individual SWNTs, the helicity of the dsDNA was able to drive the assembly of a cholesteric liquid crystal. To the authors' knowledge, this is both the first report of a lyotropic cholesteric SWNT liquid crystalline phase and one of very few systems capable of forming either cholesteric or nematic phases. The ultimate microstructure of films produced from cholesteric dispersions appears to be shear dependent. These results will enable new fundamental investigations comparing nematic and cholesteric liquid crystalline phase behavior and shear response. In addition, they potentially provide a foundation for previously unachievable applications that utilize both the intrinsic properties of SWNTs and the controlled optical properties of cholesteric films.

METHODS

Two batches of purified HiPco SWNTs were obtained: one from Rice University (Houston, TX) and the other from Unidym, Inc. (Menlo Park, CA). The purities were 99.7% and 92.0%, respectively. Lyophilized salmon testes dsDNA with 5.4% sodium salt was purchased from Sigma-Aldrich, Inc. (St. Louis, MO). The length of dsDNA fragments before and after sonication and centrifugation was measured by running dsDNA samples on 1% agarose gel in 0.5× TAE buffer with Bionexus HiLo dsDNA marker. Ethidium bromide was stained for visualization. The dsDNA fragments were determined to be double-stranded even after sonication and centrifugation using both a UV–vis absorbance spectrophotometer and fluorometric quantification. The dsDNA samples with starting concentrations of 7.5 μg/μL were diluted in TE to create different concentrations of solutions. After plating 100 μL of dsDNA samples in duplicate on a 96-well plate, 100 μL of picogreen working solution (25 μL picogreen stock in 5 mL of TE) was added to each well. The relative fluorescence units (RFU) of dsDNA assayed with picogreen reagent (Invitrogen, Cat#P11495) were measured by using SPECTRAFluor Plus fluorescence spectroscopy (TECAN, Instrument serial number 94385). RFU was normalized by subtracting off TE only (blank) RFU from all measurements before graphing.

Optical microscopy was performed on a Nikon (Melville, NY) Eclipse 80i optical microscope using precleaned glass slides and coverslips. Liquid crystal images were taken in transmission with and without cross-polarized light on a Nikon Eclipse 80i using a Plan Apo VC 60×/1.4 NA oil immersion objective; in some cases, additional magnification was used in front of the camera. Films were imaged on the same microscope using a LU Plan Fluor 20×/0.45 objective with 1.5× additional magnification in front of the camera. Rheological data were acquired on an Anton Paar (GmbH) Physica MCR 301 rheometer at 10 °C. A double gap Couette geometry was used for rheological characterization of dispersions with SWNT concentrations below 0.6 vol %; 25 mm parallel plates were used for higher concentrations. The morphology and thickness of transparent films obtained from the supernatant of concentrated dsDNA/SWNT were determined using a JEOL 7000F FE scanning electron microscope (SEM).

To calculate the volume fractions of SWNTs, 1.45 and 1.70 g/cm^3 were used as density of SWNTs and dsDNA, respectively. In a typical experiment, dsDNA was dissolved in water at 35 °C for about 45 min using a magnetic bar. The SWNTs were then added, and the mixtures were sonicated for 30 min at a power level of 50 W using a standard probe (13 mm diameter); an ice bath was used for cooling. The dsDNA/SWNTs dispersions were placed on an orbital mixer and allowed to evaporate at ambient conditions over several weeks. Samples were collected at different time intervals, and the concentrations of nanotubes were determined using an Ultrospec 2100Pro UV–vis spectrophotometer for dilute dispersions and a TA Instruments Q500 thermogravimetric analyzer under a nitrogen atmosphere for more concentrated dispersions. Care was taken to ensure that concentrations obtained by the two methods agreed for intermediate concentrations and that a mass balance was obtained. Additional information on the TGA and UV–vis spectroscopy of the dispersions may be found in the Supporting Information.

Acknowledgment. The authors acknowledge the National Science Foundation CAREER Grant CMMI-0846629 and Fluid Dynamics Grants CBET-0854010. The authors also acknowledge P. Poulin and M. Green for useful discussions.

Supporting Information Available: Information on TGA and UV–vis spectroscopy and additional cross-polarized microscopy images. This material is available free of charge *via* the Internet at http://pubs.acs.org.

REFERENCES AND NOTES

1. Nepal, D.; Balasubramanian, S.; Simonian, A. L.; Davis, V. A. Strong Antimicrobial Coatings: Single-Walled Carbon Nanotubes Armored with Biopolymers. *Nano Lett.* **2008,** *8*, 1896–1901.
2. Kang, S.; Pinault, M.; Pfefferle, L. D.; Elimelech, M. Single-Walled Carbon Nanotubes Exhibit Strong Antimicrobial Activity. *Langmuir* **2007,** *23*, 8670–8673.

3. Pangule, R. C.; Brooks, S. J.; Dinu, C. Z.; Bale, S. S.; Salmon, S. L.; Zhu, G.; Metzger, D. W.; Kane, R. S.; Dordick, J. S. Antistaphylococcal Nanocomposite Films Based on Enzyme−Nanotube Conjugates. *ACS Nano* **2010,** 874–885.
4. Shin, S. R.; Lee, C. K.; So, I. S.; Jeon, J. H.; Kang, T. M.; Kee, C. W.; Kim, S. I.; Spinks, G. M.; Wallace, G. G.; Kim, S. J. DNA-Wrapped Single-Walled Carbon Nanotube Hybrid Fibers for Supercapacitors and Artificial Muscles. *Adv. Mater.* **2008,** *20*, 466–470.
5. Collins, P. G.; Bradley, K.; Ishigami, M.; Zettl, A. Extreme Oxygen Sensitivity of Electronic Properties of Carbon Nanotubes. *Science* **2000,** *287*, 1801–1804.
6. Li, J.; Ng, H. T.; Cassell, A.; Fan, W.; Chen, H.; Ye, Q.; Koehne, J.; Han, J.; Meyyappan, M. Carbon Nanotube Nanoelectrode Array for Ultrasensitive DNA Detection. *Nano Lett.* **2003,** *3*, 597–602.
7. Tans, S. J.; Devoret, M. H.; Dai, H.; Thess, A.; Smalley, R. E.; Geerligs, L. J.; Dekker, C. Individual Single-Wall Carbon Nanotubes as Quantum Wires. *Nature* **1997,** *386*, 474–477.
8. Cao, J.; Wang, Q.; Wang, D.; Dai, H. Suspended Carbon Nanotube Quantum Wires with Two Gates. *Small* **2005,** *1*, 138–141.
9. Ericson, L. M.; Fan, H.; Peng, H.; Davis, V. A.; Zhou, W.; Sulpizio, J.; Wang, Y.; Booker, R.; Vavro, J.; Guthy, C., *et al.* Macroscopic, Neat, Single-Walled Carbon Nanotube Fibers. *Science* **2004,** *305*, 1447–1450.
10. Poulin, P.; Vigolo, B.; Launois, P. Films and Fibers of Oriented Single Wall Nanotubes. *Carbon* **2002,** *40*, 1741–1749.
11. Dalton, A. B.; Collins, S.; Munoz, E.; Razal, J. M.; Ebron, V. H.; Ferraris, J. P.; Coleman, J. N.; Kim, B. G.; Baughman, R. H. Super-Tough Carbon-Nanotube Fibres. *Nature* **2003,** *423*, 703.
12. Zhang, M.; Atkinson, K. R.; Baughman, R. H. Multifunctional Carbon Nanotube Yarns by Downsizing an Ancient Technology. *Science* **2004,** *306*, 1358–1361.
13. Vigolo, B.; Penicaud, A.; Coulon, C.; Sauder, C.; Pailler, R.; Journet, C.; Bernier, P.; Poulin, P. Macroscopic Fibers and Ribbons of Oriented Carbon Nanotubes. *Science* **2000,** *290*, 1331–1334.
14. Song, W.; Kinloch, I. A.; Windle, A. H. Nematic Liquid Crystallinity of Multiwall Carbon Nanotubes. *Science* **2003,** *302*, 1363.
15. Badaire, S.; Zakri, C.; Maugey, M.; Derre, A.; Barisci, J. N.; Wallace, G.; Poulin, P. Liquid Crystals of DNA-Stabilized Carbon Nanotubes. *Adv. Mater.* **2005,** *17*, 1673–1676.
16. Moulton, S. E.; Maugey, M.; Poulin, P.; Wallace, G. G. Liquid Crystal Behavior of Single-Walled Carbon Nanotubes Dispersed in Biological Hyaluronic Acid Solutions. *J. Am. Chem. Soc.* **2007,** *129*, 9452–9457.
17. Islam, M. F.; Alsayed, A. M.; Dogic, Z.; Zhang, J.; Lubensky, T. C.; Yodh, A. G. Nematic Nanotube Gels. *Phys. Rev. Lett.* **2004,** *92*, 88303.
18. Davis, V. A.; Ericson, L. M.; Parra-Vasquez, A. N. G.; Fan, H.; Wang, Y. H.; Prieto, V.; Longoria, J. A.; Ramesh, S.; Saini, R. K.; Kittrell, C., *et al.* Phase Behavior and Rheology of SWNTs in Superacids. *Macromolecules* **2004,** *37*, 154–160.
19. Davis, V. A.; Parra-Vasquez, A. N. G.; Green, M. J.; Rai, P. K.; Behabtu, N.; Prieto, V.; Booker, R. D.; Schmidt, J.; Kesselman, E.; Zhou, W., *et al.* True Solutions of Single-Walled Carbon Nanotubes for Assembly Into Macroscopic Materials. *Nat. Nanotechnol.* **2009,** *4*, 830–834.
20. Zakri, C.; Poulin, P. Phase Behavior of Nanotube Suspensions: From Attraction Induced Percolation to Liquid Crystalline Phases. *J. Mater. Chem.* **2006,** *16*, 4095–4098.
21. Orts, W. J.; Godbout, L.; Marchessault, R. H.; Revol, J. F. Enhanced Ordering of Liquid Crystalline Suspensions of Cellulose Microfibrils: A Small Angle Neutron Scattering Study. *Macromolecules* **1998,** *31*, 5717–5725.
22. Pan, J. H.; Hamad, W.; Straus, S. K. Parameters Affecting the Chiral Nematic Phase of Nanocrystalline Cellulose Films. *Macromolecules* **2010,** *43*, 3851–3858.
23. Davis, V. A. Liquid Crystalline Assembly of Nanocylinders. *J. Mater. Res.* **2011**in press.
24. Nepal, D.; Geckeler, K. E. Proteins and Carbon Nanotubes: Close Encounter in Water. *Small* **2007,** *3*, 1259–1265.
25. Nepal, D.; Sohn, J. I.; Aicher, W. K.; Lee, S.; Geckeler, K. E. Supramolecular Conjugates of Carbon Nanotubes and DNA by a Solid-State Reaction. *Biomacromolecules* **2005,** *6*, 2919–2922.
26. Hobbie, E. K.; Fagan, J. A.; Becker, M. L.; Hudson, S. D.; Fakhri, N.; Pasquali, M. Self-Assembly of Ordered Nanowires in Biological Suspensions of Single-Wall Carbon Nanotubes. *ACS Nano* **2009,** *3*, 189–196.
27. Onsager, L. The Effects of Shape on the Interaction of Colloidal Particles. *Ann. N.Y. Acad. Sci.* **1949,** *51*, 627–659.
28. Adams, M.; Dogic, Z.; Keller, S. L.; Fraden, S. Entropically Driven Microphase Transitions in Mixtures of Colloidal Rods and Spheres. *Nature* **1998,** *393*, 349–352.
29. Dogic, Z.; Frenkel, D.; Fraden, S. Enhanced Stability of Layered Phases in Parallel Hard Spherocylinders Due to Addition of Hard Spheres. *Phys. Rev. E* **2000,** *62*, 3925–3933.
30. Strzelecka, T. E.; Davidson, M. W.; Rill, R. L. Multiple Liquid-Crystal Phases of DNA at High-Concentrations. *Nature* **1988,** *331*, 457–460.
31. Nakata, M.; Zanchetta, G.; Chapman, B. D.; Jones, C. D.; Cross, J. O.; Pindak, R.; Bellini, T.; Clark, N. A. End-to-End Stacking and Liquid Crystal Condensation of 6 to 20 Base Pair DNA Duplexes. *Science* **2007,** *318*, 1276–1279.
32. Vanwinkle, D. H.; Davidson, M. W.; Rill, R. L. Terraces in the Cholesteric Phase of DNA Liquid-Crystals. *J. Chem. Phys.* **1992,** *97*, 5641–5646.
33. Zakharova, S. S.; Jesse, W.; Backendorf, C.; van der Maarel, J. R. C. Liquid Crystal Formation in Supercoiled DNA Solutions. *Biophys. J.* **2002,** *83*, 1119–1129.
34. Sipski, M. L.; Wagner, T. E. Probing DNA Quaternary Ordering with Circular-Dichroism Spectroscopy—Studies of Equine Sperm Chromosomal Fibers. *Biopolymers* **1977,** *16*, 573–582.
35. Livolant, F. Cholesteric Organization of DNA *In Vivo* and *In Vitro*. *Eur. J. Cell Biol.* **1984,** *33*, 300–311.
36. Rill, R. L.; Livolant, F.; Aldrich, H. C.; Davidson, M. W. Electron-Microscopy of Liquid-Crystalline DNA—Direct Evidence for Cholesteric-like Organization of DNA in Dinoflagellate Chromosomes. *Chromosoma* **1989,** *98*, 280–286.
37. Sinden, R. R. *DNA Structure and Function*; Academic Press: San Diego, CA, 1994; pp 34−37.
38. Singer, V. L.; Jones, L. J.; Yue, S. T.; Haugland, R. P. Characterization of Picogreen Reagent and Development of a Fluorescence-Based Solution Assay for Double-Stranded DNA Quantitation. *Anal. Biochem.* **1997,** *249*, 228–238.
39. O'Connell, M. J.; Bachilo, S. M.; Huffman, C. B.; Moore, V. C.; Strano, M. S.; Haroz, E. H.; Rialon, K. L.; Boul, P. J.; Noon, W. H.; Kittrell, C., *et al.* Band Gap Fluorescence from Individual Single-Walled Carbon Nanotubes. *Science* **2002,** *297*, 593–596.
40. Girifalco, L. A.; Hodak, M.; Lee, R. S. Carbon Nanotubes, Buckyballs, Ropes, and a Universal Graphitic Potential. *Phys. Rev. B* **2000,** *62*, 13104–13110.
41. Doi, M.; Edwards, S. F. *The Theory of Polymer Dynamics*; Oxford University Press: Oxford, 1986.
42. Song, W.; Windle, A. H. Isotropic-Nematic Phase Transition of Dispersions of Multiwall Carbon Nanotubes. *Macromolecules* **2005,** *38*, 6181–6188.
43. Donald, A. M.; Windle, A. H.; Hanna, S. *Liquid Crystalline Polymers*; Cambridge University Press: New York, 2006; pp 244−255.
44. Stanley, C. B.; Hong, H.; Strey, H. H. DNA Cholesteric Pitch as a Function of Density and Ionic Strength. *Biophys. J.* **2005,** *89*, 2552–2557.
45. Kornyshev, A. A.; Leikin, S. Electrostatic Interaction between Long, Rigid Helical Macromolecules at all Interaxial Angles. *Phys. Rev. E* **2000,** *62*, 2576–2596.
46. Kornyshev, A. A.; Leikin, S.; Malinin, S. V. Chiral Electrostatic Interaction and Cholesteric Liquid Crystals of DNA. *Eur. Phys. J. E* **2002,** *7*, 83–93.

47. Nicolosi, V.; Cathcart, H.; Dalton, A. R.; Aherne, D.; Dieckmann, G. R.; Coleman, J. N. Spontaneous Exfoliation of Single-Walled Carbon Nanotubes Dispersed Using a Designed Amphiphilic Peptide. *Biomacromolecules* **2008,** *9*, 598–602.
48. Vollrath, F.; Knight, D. P. Liquid Crystalline Spinning of Spider Silk. *Nature* **2001,** *410*, 541–548.
49. Larson, R. G. *The Structure and Rheology of Complex Fluids*; Oxford University Press: New York, 1999; pp 476−478.
50. Lee, S. W.; Wood, B. M.; Belcher, A. M. Chiral Smectic C Structures of Virus-Based Films. *Langmuir* **2003,** *19*, 1592–1598.